



Publication Year	2019
Acceptance in OA @INAF	2021-02-25T10:51:05Z
Title	Conditions for the Long-Term Preservation of a Deep Brine Reservoir in Ceres
Authors	Castillo-Rogez, Julie C.; Hesse, M. A.; FORMISANO, Michelangelo; Sizemore, H.; Bland, M.; et al.
DOI	10.1029/2018GL081473
Handle	http://hdl.handle.net/20.500.12386/30609
Journal	GEOPHYSICAL RESEARCH LETTERS
Number	46

**1 Conditions for the Long-Term Preservation of a Deep
2 Brine Reservoir in Ceres**

Julie C. Castillo-Rogez¹, M. A. Hesse², M. Formisano³, H. Sizemore⁴, M.

Bland⁵, A. I. Ermakov¹, R. R. Fu⁶

J. C. Castillo-Rogez, Jet Propulsion Laboratory, 4800 Oak Grove Drive, Pasadena, CA 91109,
USA (Julie.C.Castillo@jpl.nasa.gov.)

¹Jet Propulsion Laboratory, California
Institute of Technology, Pasadena, CA,
United States

²The University of Texas at Austin,
Department of Geological Sciences, Austin,
TX, United States

³INAF-IAPS, Istituto di Astrofisica e
Planetologia Spaziali di Roma, Italy

⁴Planetary Science Institute, Tucson, AZ,
United States

⁵United States Geological Survey,
Flagstaff, AZ, United States

⁶Department of Earth and Planetary
Sciences, Harvard University, Cambridge,
MA, United States

3 Abstract: We propose a new internal evolution model for the dwarf planet
4 Ceres matching the constraints on Ceres' present internal state from the Dawn
5 mission observations. We assume an interior differentiated into a volatile-dominated
6 crust and rocky mantle, and with remnant brines in the mantle, all consis-
7 tent with inferences from the Dawn geophysical observations. Simulations
8 indicate Ceres should preserve a warm crust until present if the crust is rich
9 in clathrate hydrates. The temperature computed at the base of the crust
10 exceeds 220 K for a broad range of conditions, allowing for the preservation
11 of a small amount of brines at the base of the crust. However, a tempera-
12 ture ≥ 250 K, for which at least 1 wt.% sodium carbonate gets in solution
13 requires a crustal abundance of clathrate hydrates greater than 55 vol.%, a
14 situation possible for a narrow set of evolutionary scenarios.

1. Introduction

15 Per its combination of chemical, physical, and geological observations on global, re-
16 gional, and local scales, the Dawn mission has provided the most extensive dataset for an
17 ice-rich body (Russell et al. 2016). Ceres is a 940-km large body with a mean density
18 of 2162 kg/m^3 (Park et al. 2016). This corresponds to an ice to anhydrous rock ratio
19 of 47:53 in volume or 25:75 in mass. Hence its evolution is driven by the interplay of
20 radiogenic heating with the thermodynamic and mechanical properties of water and hy-
21 drates. Observational constraints returned by the Dawn mission are summarized in recent
22 studies (e.g., McCord and Castillo-Rogez 2018). The geophysical properties this study
23 aims to match are summarized in Section 2. They include constraints on the properties of
24 the upper 100 km, in particular composition and viscosity profile. An important feature
25 derived from Dawn’s observations is a rapid decrease in viscosity within the uppermost
26 40 km and persistent low viscosities at about 10^{21} Pa s below and at least down to 100
27 km depth. This has been interpreted by the presence of a few vol.% pore fluid (Fu et
28 al. 2017). Our objective is to determine what set of starting conditions and assump-
29 tions on the properties of the crust and potassium distribution enable the preservation
30 of fluids at about 40 km depth until present. Methods are presented in Section 3 and
31 results in Section 4. These results provide thermal context for various processes whose
32 occurrence has been suggested for Ceres, in particular the prospect for cryovolcanism and
33 the development of cryomagma reservoirs upon impact heating in the crust (Hesse and
34 Castillo-Rogez, in revisions) (Section 5). In turn, this study brings new insights into the

35 internal evolution of a body, which, from a geophysical standpoint, is relevant to other
36 dwarf planets and midsized icy moons.

2. Constraints on Ceres' Interior from Dawn

37 In the course of two years of orbital mapping, the Dawn mission returned images, near-
38 infrared spectra, and gravity measurements of Ceres on a global scale and for a wide
39 range of illuminations. Gravity data yielded a normalized mean moment of inertia of
40 about 0.37 pointing to partial differentiation (Park et al. 2016). Admittance analysis
41 provided additional constraints on crustal properties, which is 40 km thick on average
42 with a density of 1200 to 1400 kg/m³ (assuming a two layer model, Ermakov et al. 2017).
43 The crust overlays a mantle with a density of ~ 2400 kg/m³ and a viscosity lower than 10^{21}
44 Pa s, which Fu et al. (2017) interpreted as evidence for a small amount of pore fluid. The
45 nature of the fluid is not constrained but it could realistically be sodium and potassium
46 chloride brines as suggested by geochemical modeling (Neveu and Desch 2015; Castillo-
47 Rogez et al. 2018). The brines likely correspond to residual liquid from the freezing of a
48 global ocean suggested in Ceres early on (Castillo-Rogez and McCord 2010; Ammannito
49 et al. 2016). The eutectic temperature of that brine could be as low as about 220 K
50 (Castillo-Rogez et al. 2018). Ammonia could also be present and decrease the eutectic
51 further. However, the widespread occurrence of ammonium both in the form of clays
52 and salts on Ceres' surface indicates these formed in an environment where ammonia was
53 a minor component. Following Le Chatelier's Principle, most of the ammonia should be
54 turned into ammonium since the latter was removed from the medium, either by exchange
55 with cations in clays or by salt precipitation.

56 Extensive evidence for the occurrence of salt compounds in Ceres' crust is expressed in
57 the form of many sites enriched in carbonates and ammonium chlorides (De Sanctis et
58 al. 2016, 2018). These species are likely associated with other chlorides, like hydrohalite
59 (Castillo-Rogez et al. 2018) that cannot be detected by Dawn's instruments. Brines
60 are believed to play a role in the emplacement of two outstanding geological landmarks:
61 Ahuna Mons (Ruesch et al. 2016) and the bright material (faculae) in Occator crater (De
62 Sanctis et al. 2016; Quick et al. 2019). Both constructs display sodium carbonate (De
63 Sanctis et al. 2016 for the Occator faculae and Zambon et al. 2017 for Ahuna Mons).
64 The deep brine layer identified by Fu et al. (2017) has been suggested as a reservoir for
65 the Occator faculae (Quick et al. 2019).

66 Additional constraints on Ceres' crustal composition come from its mechanical strength,
67 which Bland et al. (2016) found to be at least three orders of magnitude greater than
68 ice for Ceres' temperatures. It suggests no more than 40 vol.% of a weak phase, which
69 Bland et al. (2016) interpreted as an upper bound on the water ice fraction. That fraction
70 could be less if the crust also contains porosity. The extent of porosity is not constrained
71 though and might show lateral variations, as indicated by the distribution of surface
72 fractures (Scully et al. 2017).

73 Strong phases are required to reproduce the strength of the crust, which Fu et al.
74 (2017) inferred to be a mixture of phyllosilicates, salt hydrates and gas hydrates (i.e.,
75 clathrate hydrates). The latter are likely to be mixed methane and carbon dioxide hy-
76 drates (Castillo-Rogez et al. 2018) with a density of about 1000 kg/m^3 (e.g., Waite et
77 al. 2007). Geochemical modeling suggests there should be no more than 20 vol.% salts in

78 the crust and the averaged density of these salts, composed of carbonates and chlorides
79 is about 2200 kg/m^3 (Castillo-Rogez et al. 2018). In this framework, phyllosilicates are a
80 mixture of magnesium serpentine and clays, in particular saponite, consistent with surface
81 composition (De Sanctis et al. 2015). A mixture of 10 vol.% silicates, 20 vol.% hydrated
82 salts, and 30 vol.% ice and 40 vol.% clathrates matches the average crustal density derived
83 by Ermakov et al. (2017) and is consistent with the strength estimates from Bland et al.
84 (2016) and Fu et al. (2017).

85 Ceres' crust relaxes on scales greater than $\sim 250 \text{ km}$, which Fu et al. (2017) inter-
86 preted with a crustal viscosity profile decreasing by one order of magnitude every 10 km.
87 Formisano et al. (2018) used a 2-D finite element numerical code to solve the thermal
88 convection equations in the Boussinesq approximation and explore the onset of subsolidus
89 thermal convection in the crust (40 km thick shell) of Ceres. They found that no thermal
90 convection is possible, assuming less than 40vol.% of weak material (Bland et al. 2016).
91 Convection may be possible if the ice content is slightly greater than 40% and the tem-
92 perature at the base of the crust ranges from 250 to 300 K. Strong thermal convection
93 is possible if 50vol.% of ice is assumed, leading to a Rayleigh number greater than 10^8 .
94 However, as shown below, the modeled temperatures at the base of the crust are expected
95 to be colder than required for convection to be initiated throughout Ceres' history.

3. Modeling Approach

96 This paper follows the one-dimensional thermal modeling approach by Castillo-Rogez
97 and Lunine (2010). We account for the redistribution of potassium following leaching from
98 the silicates upon aqueous alteration. This process is promoted in presence of ammonium

99 whose exchange with potassium and sodium is enhanced at temperature below 50° C
100 (Neveu et al. 2017). In Castillo-Rogez et al. (2018), potassium accumulates with chlorine
101 and sodium in the residual liquid layer at the base of the crust. The distribution of this
102 brine may encompass a few tens of kilometers in the upper part of the mantle or a larger
103 area depending on porosity. We vary the fraction of potassium leached from the rock from
104 10 to 90% and redistributed it in the brine layer in the upper part of the mantle, down
105 to the 100 km depth (i.e., the upper 60 km of the mantle) that could be probed by the
106 Fu et al. (2017) modeling.

107 Ceres is assumed to form about 3.5 Ma after the condensation of calcium and aluminum
108 rich inclusions (CAI) , which define the starting concentrations of ^{26}Al in Ceres. The exact
109 time of formation is not important for this study as long as there is enough ^{26}Al to drive
110 global melting and differentiation following formation. For times of formation later than 5
111 Ma after CAIs, Castillo-Rogez and McCord (2010) found that Ceres could preserve a thick
112 (>150 km) crust of its original composition, presumably of dry rock. This situation is
113 not consistent with the Dawn observations, both in terms of surface composition, crustal
114 density, and moment of inertia and we do not cover it in the present study.

115 Freezing occurs top down and results in the development of a crust that is ice rich. Mod-
116 eling of the freezing of the ocean with FREZCHEM yields salts and clathrates (Castillo-
117 Rogez et al. 2018). Clathrates may represent the dominant form of water at pressures of a
118 few MPa. Hence the crustal composition may range from the minimal 30 vol.% clathrates
119 required by the observations (on top of silicates and hydrated salts) up to 70 vol.%. The
120 thermal conductivity of the mixture, K_{crst} , is the sum of the component conductivities

121 weighted by their volume fractions. It ranges from about 0.6 W/m/K for 0 vol.% ice (i.e.,
122 70 vol.% clathrates) to 2.0 W/m/K for 55 vol.% ice. Silicates are a minor component of
123 the mixture, and thus their impact on the thermal conductivity is small. This modeling
124 does not account for organics, which might be abundant in the crust (Marchi et al. in
125 press). Organics are diverse and their densities cover a broad range, but their abundance
126 in Ceres' crust is not constrained.

127 Settling of phyllosilicates upon melting of the ice is assumed to proceed to near com-
128 pletion. That is, we do not model a mudball interior, in which silicate grains remain in
129 suspension with a fluid phase throughout much of the early mantle. The crustal density
130 predicted by Travis et al. (2018) for a mudball interior is broadly consistent with the den-
131 sity inferred from a two-layer gravity model (1450 vs 1290 kg/m³; Ermakov et al. 2017).
132 The difference might be due to different assumptions on the fraction of rocky particles
133 that can remain in suspension in the ocean. For example ionic charging, a common phe-
134 nomenon observed in marine clays (e.g., Sutherland et al. 2015) could play a major role in
135 driving particle settling, or flocculation, as the ocean freezes and thus salinity increases.
136 Furthermore, muddy sediment is difficult to erode and resuspend (Hjulstroem 1935). The
137 mudball model predicts the long-term preservation of hundreds of kilometers of liquid in-
138 side Ceres at present and, presumably, could match the mechanical constraints derived by
139 Fu et al. (2017). Our admittedly simpler model yields higher heat flow and thus provides
140 a bound on the maximum temperatures that can be reached in Ceres at present. So,
141 the two approaches may be viewed as two endmember evolutionary pathways for Ceres.
142 Lastly, the concentration of metal-rich, i.e., dense, particles toward the center cannot be

143 ruled out (King et al. 2018). However, the extent of that process is unconstrained, so
144 this study assumes a simple three-layer structure (mantle, briny mud, crust) for Ceres'
145 interior.

146 Material properties are gathered in the Supplement. For the initial concentration in
147 long-lived radioisotopes, we chose a mean carbonaceous chondrite composition character-
148 ized by an average potassium content of $\sim 500\text{-}550 \mu\text{g g}^{-1}$ (Lodders 2003). Oceanic muds
149 have a thermal conductivity from 0.5 to $\sim 1.5 \text{ W/m/K}$ depending on the relative fractions
150 of particles, brine, gas, and gas hydrates (e.g., Camerlenghi et al. 1995; Muraoka et al.
151 2014). Serpentine has a thermal conductivity of about 2.5 W/m/K while anhydrous sili-
152 cates (olivine and pyroxene) have thermal conductivities up to 5 W/m/K (see Opeil et al.
153 2010 for a review). The latter could be present if aqueous alteration was partial. Also, the
154 presence of iron-rich compounds in the rock (like iron sulfide and oxides) could increase
155 the thermal conductivity further. In this study, we cover a range of thermal conductivities
156 for the mantle from 0.5 to 2.5 W/m/K under the assumption that aqueous alteration was
157 advanced, as suggested by the Dawn observations (e.g., De Sanctis et al. 2018).

4. Representative Interior Evolution Models Consistent with Dawn's Observations

158 The model presented in Figure 1a is characterized by a mantle thermal conductivity
159 of 1.5 W/m/K , a crust thermal conductivity of 1.1 W/m/K , and assumes 50% of the
160 potassium has been leached from the silicates and is stored in remaining liquid at the top
161 (60 km) of the mantle. In these conditions, the mantle remains cold and never reaches the

162 dehydration temperature of serpentine and clays, around 800 K. This is consistent with
163 the gravity constraints from Ermakov et al. (2017).

164 Figure 1b shows the heat flow history for that model. Due to the low conductivity of
165 the core and the insulating effect of the crust, heat leaks out slowly. It slowly decreases
166 over time, from ~ 3 mW/m² 1 Ga after formation to ~ 2.1 mW/m² for present time.

167 Trends in parametric dependence (Figure 2) show that the key parameter determining
168 the temperature at the base of the crust is, as expected, the crustal thermal conductivity.
169 The mantle thermal conductivity, which determines the heat flowing from the mantle
170 to the crust, further contributes to warming the base, although its impact is at most 12
171 degrees over a factor five increase. Hence, efficient heat transfer from the mantle combined
172 with an insulating effect of the crust results in trapping heat at the base of the crust and
173 yields temperatures above 220 K (i.e., the eutectic of the chloride brine mixture) for a
174 large space of conditions, specifically if $K_{crst} \leq \sim 1.4$ W/m/K. The crust-mantle interface
175 temperature reaches the water eutectic for $K_{crst} \leq 0.8$ W/m/K, whereas an ice-dominated
176 crust with a thermal conductivity ≥ 1.6 W/m/K would not allow temperatures warm
177 enough for brines to persist until present.

178 The contribution of the displacement of ⁴⁰K from the rock to a brine layer at the top of
179 the mantle results in increasing the temperature at the interface with the crust by only a
180 few degrees.

181 A low value of K_{crst} can be explained if the crust is enriched in hydrates, such as
182 clathrate hydrates. A conductivity of 1.4 W/m/K corresponds to about 40 vol.%, which,
183 combined with 20 vol.% salts and 10 vol.% silicates (to meet the observed crustal density),

184 is consistent with the crustal strength derived by Bland et al. (2016). A value of 0.8
185 W/m/K, requires ~ 65 vol.% clathrate hydrates, which is theoretically possible but implies
186 that clathrate hydrates formed during the freezing of the ocean avoided destabilization
187 from impacts until. This scenario is hard to reconcile with Ceres' impacting history and
188 with regional evidence for increased ice content in the crust (Sizemore et al., in press.)
189 On the other hand, $K_{crst} \geq 1.6$ W/m/K, the condition for Ceres to be entirely frozen
190 at present, implies an abundance of clathrates $\leq 30\%$, which is also a plausible scenario.
191 Increased abundance of silicates with respect to hydrated salts, two high strength materials
192 of similar densities but contrasting thermal conductivities, can further act in increasing
193 thermal conductivity.

194 Temperatures in the modeled mantle exceed the dehydration temperature of hydrated
195 silicates when the average $K_{mtl} \leq 1.2$ W/m/K. The mantle density inferred by Ermakov
196 et al. (2017) indicates little or not hydration of the silicates. It is possible an enrichment
197 in metal-rich particles with depth increases the thermal conductivity of the mantle. An
198 alternative explanation is that hydrothermal circulation could still be ongoing in fractures,
199 enhancing heat transfer and thus the effective thermal conductivity of the medium (Neveu
200 et al. 2015).

201 The amount of remaining liquid vs. temperature for the mix of salts predicted by
202 Castillo-Rogez et al. (2018) is presented in Figure 3a. The remaining liquid fraction
203 represents $\leq 2\%$ of the original ocean for temperatures below ~ 248 K and $\leq 1\%$ below
204 ~ 244 K. At 220 K, only 0.4% of the original ocean remains. Assuming that all of Ceres'
205 volatile content melted as a consequence of short-lived radioisotope decay (Castillo-Rogez

206 and McCord, 2010), these fractions correspond to a global layer between 200 m and 1000
207 m thick. However, below the crust, this liquid is likely distributed in a matrix of silicates
208 and other solid materials in the form of pore (interstitial) fluid down to at least 100 km
209 depth. Further modeling is required to determine the distribution of the liquid based on
210 the expected matrix properties (e.g., porosity and permeability).

5. Implications and Discussion

211 Our modeling shows that it is realistic from a thermal standpoint to expect at least a
212 few percent of brines (in volume) to be preserved in Ceres' mantle until present, provided
213 that the crust is enriched in insulating material such as clathrates. Clathrates have also
214 been suggested as responsible for the inferred low density and high mechanical strength of
215 the crust (Bland et al. 2016; Fu et al. 2017) and are predicted to be a dominant species
216 from geochemical modeling (Castillo-Rogez et al. 2018). In these conditions, heat flowing
217 from Ceres' crust can be slightly lower than incoming heat from the rocky mantle, which
218 contributes to the long term preservation of liquid. However, unless the crust is dominated
219 by clathrates, Ceres is on the edge of being completely frozen, which is also consistent
220 with Neveu and Desch (2015). On the other hand, as noted above, our modeling approach
221 potentially yields an conservative case where modeling Ceres as a mudball (Travis et al.
222 2018) could be more appropriate. The bottom line is that the preservation of liquid inside
223 Ceres until present is expected for a wide range of thermal evolution scenarios.

224 *Lateral Variations in Crustal Properties:* Sizemore et al. (2018) inferred from Ceres'
225 geology lateral variations in ice content across Ceres. In particular, the Hanami Planum
226 region displays Ceres' most ancient terrains and mildly relaxed geological features in com-

227 parison to the surrounding planitiae. Most of the craters with central pits are concentrated
228 in this region. Hanami Planum is also characterized by a thicker crust than average (~ 50
229 km, Ermakov et al. 2017). A possible interpretation is that this old region has preserved a
230 substantial fraction of clathrates with respect to the planitiae that might represent basins
231 created by large impacts (Marchi et al. 2016). Combining a thicker crust with a low
232 thermal conductivity could then lead to locally warmer temperatures and thus increased
233 abundance in liquid at the base of the crust. Preliminary estimates from this modeling
234 suggest the base of Hanami Planum could be ~ 5 - 10 K warmer than the average basal
235 temperature. However, more advanced two- or three- dimensional thermal modeling is
236 required for a more accurate estimate.

237 The topography relaxation study by Fu et al. (2017) cannot resolve regional varia-
238 tions in viscosity contrast between the crust and mantle. Impact-induced variations in
239 clathrate abundance in the crust could locally shift the crustal thermal conductivity from
240 ~ 1 W/m/K to up to 2.4 W/m/K, with potential signatures in the geology that remain
241 to be explored.

242 *Prospect for Cryovolcanism:* The occurrence of sodium carbonate at both the Occator
243 faculae and Ahuna Mons requires the sources of the constructs to be warm enough for
244 that compound to be in solution. The fluid does not require a large concentration of
245 sodium carbonate though, since the bulk of the Occator dome and of Ahuna Mons could
246 be built from a different material, for example ice shielded from sublimation by a thin
247 crust of carbonate and chlorides.

248 For our average model, the fraction of NaHCO_3 in solution is only 0.1 wt.% at 245
249 K (Figure 5b). Temperatures in excess of 250 K are required for several percent of
250 that compound to be in solution. Such warm temperatures could be met below Hanami
251 Planum, as noted in the previous subsection. Sodium carbonate is a minor component
252 of the salt inventory modeled for Ceres (e.g., in comparison to the chlorides) and is
253 predicted to be among the first salts incorporated in the crust (Castillo-Rogez et al.
254 2018). Thus, the extent to which the deep brine layer could represent a major reservoir
255 of sodium carbonate for the Occator faculae is uncertain. An alternative, and potentially
256 complementary scenario is that geological activity associated with Occator and other
257 large craters (in the past) was in part driven by the heat produced upon impacting, as
258 an additional way to inject heat into the crust and put in solution sodium carbonates
259 already present in the crust (Castillo-Rogez et al. 2018) A hybrid model combining both
260 impact-generated melt and a deeper source is another possibility (see next subsection).

261 Ahuna Mons, a ~ 4 -km high by 17-km wide construct, sits on a ~ 40 km thick crust,
262 similar to our modeling assumption, i.e., temperatures colder than 245 K are expected at
263 the base of the crust. Even in the most optimistic case, the bottom heat flow is lower than
264 3 mW/m^2 , insufficient to drive convective upwelling (Formisano et al., 2018). The lack of
265 flexural deformation associated with the mons further indicates a low heat flow. Instead,
266 Neveu and Desch (2015) suggested that expressions of volcanism on Ceres' surface, such
267 as Ahuna Mons, could be the result of passive upwelling of mantle material due to volume
268 changes in a freezing interior. However, a model that reconciles both mineralogy and
269 geophysics remains to be pursued.

270 *Thermal Context for Impact Melt Production:* In the case of the Occator faculae, a
271 cryomagma reservoir produced by impact heat (Bowling et al. 2019; Hesse and Castillo-
272 Rogez, in revisions) can reach the required temperature for a significant fraction of crustal
273 sodium carbonate to get in solution and contribute to the bulk of the facula carbonates as
274 the solution is brought to the surface from freezing stresses (following a similar process as
275 described in Quick et al. 2019). The thermal gradient inferred from our modeling (which
276 favors a certain temperature at the base of the crust), is at least 4 times steeper than the
277 thermal gradient assumed by Bowling et al. (2019) in their modeling of the evolution of
278 the melt reservoir created by the impact that created Occator crater. A different thermal
279 background can have a significant effect over the lifetime of that melt, as pointed out by
280 these authors and demonstrated by Hesse and Castillo-Rogez (in revisions). The latter
281 authors show that the impact-produced melt reservoir could survive up beyond 10 Ma
282 and potentially still be a source for the recent exposure of brines, depending on the size
283 of the impact melt chamber. Our modeling can also be used to compute the amount and
284 depth of melt produced by impacts throughout Ceres' history.

6. Summary

285 The preservation of a relict ocean in Ceres until present is possible provided that the
286 thermal conductivity of the crust is less than 1.4 W/m/K. This value is consistent with
287 that expected for the mixture of ice and hydrated materials (especially salts and clathrate
288 hydrates) inferred from geophysical observations (Bland et al. 2016; Fu et al. 2017).
289 A moderate rocky mantle thermal conductivity ($\sim 1 - 2$ W/m/K) further contributes
290 to the preservation of a warm brine layer at the base of the crust. On the other hand,

291 the displacement of ^{40}K from the rock to the salts has a relatively minor impact on
292 Ceres' crustal temperature. The water ice eutectic is reached if the crust is dominated
293 by clathrate hydrates in excess of 65 vol.%. On the other hand, the prospect of liquid at
294 shallow depth, as depicted in Nathues et al. (2017) and Stein et al. (2017), is unlikely
295 based on our geophysical modeling. This implies that the exposure of salts from a brine
296 reservoir is a phenomenon that might be limited to impacts large enough to connect
297 with the deep brine layer (e.g., via the introduction of fractures) and/or to create a local
298 melt reservoir (Bowling et al. 2019; Hesse and Castillo-Rogez, in revisions). Conversely,
299 the warm thermal background created by a large abundance of hydrates in the crust
300 implies that brine-driven activity following large impacts must have been common in
301 Ceres' history, as illustrated by the many occurrences of salt deposits associated with
302 fracture networks in large craters (Buczowski et al. 2018; Azacca Crater, Dantu Crater).
303 Clathrates may further contribute to that process by supplying gas when destabilized and
304 increasing melt buoyancy (e.g., Quick et al. 2019).

305 One cannot exclude that warmer basal temperatures could be reached locally, for ex-
306 ample below Hanami Planum's thick crust. Conversely, local conversion of clathrates into
307 ice by large impacts could increase the average crust thermal conductivity, with possible
308 expressions in the surface morphology. Two- or three-dimensional thermal modeling is
309 required to explore the evolution of Ceres' complex crust for comparison against surface
310 features.

311 **Acknowledgments.** Part of this work has been conducted at the Jet Propulsion Lab-
312 oratory, California Institute of Technology, under a contract with NASA. All rights re-
313 served. Government sponsorship acknowledged.

References

- 314 Ammannito, E., De Sanctis, M. C., Ciarniello, M., Frigeri, A., Carrozzo, F. G., Combe,
315 J.-Ph., Ehlmann, B. E., et al. (2016) Distribution of ammoniated magnesium phyllosil-
316 icates on Ceres, *Science* 353, aaf4279.
- 317 Bland, M. T., Raymond, C. A., Fu, R. R., Schenk, P., Kneissl, T., Pasckert, J.H.,
318 Hiesinger, H., Preusker, F., Park, R., Marchi, S., King, S., Castillo-Rogez, J. C., Rus-
319 sell, C.T. (2016), Composition and structure of the shallow subsurface of Ceres revealed
320 by crater morphology, *Nature Geoscience* 9, 538-542.
- 321 Bland, M. T., Sizemore, H. G., Buczkowski, D. L., Sori, M. M., Raymond, C. A., King,
322 S. D., Russell, C. T. (2018a) Why is Ceres Lumpy? Surface Deformation Induced
323 by Solid-State Subsurface Flow, 49th Lunar and Planetary Science Conference 19-23
324 March, 2018, held at The Woodlands, Texas LPI Contribution No. 2083, id.1627
- 325 Bland, M. T., Ermakov, A. I., Raymond, C. A., Williams, D. A., Bowling, T. J., Preusker,
326 F., Park, R. S., Marchi, S., Castillo-Rogez, J. C., Fu, R. R., Russell, C. T. (2018b)
327 *Geophys. Res. Lett.* 45, 1297-1304.
- 328 Bowling, T. J., Ciesla, F. J., Davison, T. M., Scully, J. E. C., Castillo-Rogez, J. C.,
329 Marchi, S., Post-Impact Thermal Structure and Cooling Timescales of Occator Crater
330 on Asteroid 1 Ceres, *Icarus*, <https://doi.org/10.1016/j.icarus.2018.08.028>.

- 331 Buczkowski, D. L., Sizemore, H. G., Bland, M. T., Scully, J. E. C., Quick, L. C.,
332 Hughson, K. H. G., Park, R., Preusker, F., Raymond, C. A., Russell, C. T. (2018)
333 Floor?Fractured Craters on Ceres and Implications for Interior Processes, *J. Geophys.*
334 *Res.*, <https://doi.org/10.1029/2018JE005632>.
- 335 Camerlenghi, A., Cita, M. B., Della Vedova, B., Fusi, N., Mirabile, L., Pellis, G. (1995)
336 Geophysical evidence of mud diapirism on the Mediterranean Ridge accretionary com-
337 plex, *Marine Geophysical Researches* 17, 115-141.
- 338 Castillo-Rogez, J. C., Lunine, J. I. (2010) Evolution of Titan's rocky core con-
339 strained by Cassini observations, *Geophysical Research Letters* 37, L20205, doi:
340 doi:10.1029/2010GL044398.
- 341 Castillo-Rogez, J. C., McCord, T. B. (2010) Ceres' evolution and present state constrained
342 by shape data, *Icarus* 205, 443-459, doi:10.1016/j.icarus.2009.04.008.
- 343 Castillo-Rogez, J. C., Neveu, M., McSween, H. Y., Fu, R. R., Toplis, M., Prettyman,
344 T. H. (2018) Insights into Ceres' evolution from surface composition, *Meteoritics and*
345 *Planetary Science* 53, 1820-1843.
- 346 Dai, S., Cha, J.-H., Rosenbaum, E. J., Zhang, W., Seol, Y. (2015) Thermal conductivity
347 measurements in unsaturated hydrate-bearing sediments, *Geophys. Res. Lett.* 42, 6295-
348 6305, doi:10.1002/2015GL064492.
- 349 De Sanctis, M. C., Ammanito, E., Raponi, E., Marchi, S., Mcord T. B., et al. (2015)
350 Ammoniated phyllosilicates with a likely outer Solar system origin on (1) Ceres, *Nature*
351 528, 241-244.

- 352 De Sanctis, M.C., Raponi, A., E. Ammannito, M. Ciarniello, M.J. Toplis, H.Y. McSween,
353 J.C. Castillo-Rogez, B.L. Ehlmann, F.G. Carrozzo, S. Marchi, F. Tosi, F. Zambon,
354 F. Capaccioni, M.T. Capria, S. Fonte1, M. Formisano, A. Frigeri, M. Giardino, A.
355 Longobardo, G. Magni, E. Palomba, L.A. McFadden, C.M. Pieters, R. Jaumann, P.
356 Schenk, R. Mugnuolo, C.A. Raymond, C.T. Russell (2016) Bright carbonate deposits
357 as evidence of aqueous alteration on (1) Ceres, *Nature* 536, 54-57.12
- 358 Engel, S., J. I. Lunine, and D. L. Norton (1994) Silicate interactions with ammonia-water
359 fluids on early Titan, *J. Geophys. Res.* 99 (E2), 3745-3752.
- 360 Ermakov, A. I., Fu, R. R., Castillo-Rogez, J. C., Raymond, C. A., Park, R. S., Preusker,
361 F., Russell, C. T., Smith, D. E., Zuber, M. T., Constraints on Ceres' internal structure
362 and evolution from its shape and gravity measured by the Dawn spacecraft, *J. Geophys.*
363 *Res.* 122, 2267-2293.
- 364 Formisano, M., Costanzo, F., Magni, G., De Sanctis, M. C. (2018) (1) Ceres: Study of
365 Thermal Convection in the Mantle and its Mechanical Effects, 42nd COSPAR Scientific
366 Assembly. Held 14-22 July 2018, in Pasadena, California, USA, Abstract id. B1.1-20-18.
- 367 Fu, R. R., Ermakov, A., Marchi, S., Castillo-Rogez, J. C., and 8 co-authors, Interior
368 structure of the dwarf planet Ceres as revealed by surface topography, *EPSL* 476, 153-
369 164.
- 370 Glein, C. R., Shock, E. L. (2010) Sodium chloride as a geophysical probe of a subsurface
371 ocean on Enceladus, *Geophys. Res. Lett.* 37, L09204.
- 372 Hayne, P. O., Aharonson, O. (2015) Thermal stability of ice on Ceres with rough topog-
373 raphy, *J. Geophys. Res.* 120, 1567-1584.

- 374 Hesse, M., Castillo-Rogez, J. C., Thermal evolution of the impact-induced cryomagma
375 chamber beneath Occator Crater on Ceres, *Geophys. Res. Lett.*, submitted (provided
376 with submission).
- 377 Hjulstrom, F. (1935). Studies of the morphological activity of rivers as illustrated by the
378 River Fyris, *Bulletin. Geological Institute Upsalsa*, 25, 221-527.
- 379 King S. D., Castillo-Rogez J. C., Toplis M. J., Bland M. T., Raymond C. A., and Russell C.
380 T. 2018. Ceres internal structure from geophysical constraints. *Meteoritics & Planetary*
381 *Science*. <https://doi.org/10.1111/maps.13063>.
- 382 Kirk, R. L. and D. J. Stevenson (1987) Thermal evolution of a differentiated Ganymede
383 and implications for surface features, *Icarus* 69, 91-134.
- 384 Lodders, K. (2003) Solar System Abundances and Condensation Temperatures of the
385 Elements, *The Astrophysical Journal* 591, 1220, doi:10.1086/375492.
- 386 Marchi, S., Ermakov, A. I., Raymond, C. A., Fu, R. R., O'Brien, D. P., Bland, M. T.,
387 Ammannito, E., De Sanctis, M. C., Bowling, T., Schenk, P., Scully, J. E. C., Buczkowski,
388 D. L., Williams, D. A., Hiesinger, H., Russell, C. T. (2016) The missing large impact
389 craters on Ceres, *Nature Communications* 7, Article number: 12257.
- 390 Marchi, S., Raponi, A., Prettyman, T., De Sanctis, M. C., Castillo-Rogez, J., Raymond,
391 C., Ammannito, E., Bowling, T., Ciarniello, M., Kaplan, H., Palomba, E., Russell,
392 C., Vinogradoff, V., Yamashita, N., An aqueously altered carbon-rich Ceres, *Nature*
393 *Astronomy*, in press (embargoed until December 10).
- 394 McCord T. B. and Castillo-Rogez J. C. (2018). Ceres's internal evolution: The view after
395 Dawn. *Meteoritics & Planetary Science*. <https://doi.org/10.1111/maps.13135>.

- 396 Muraoka, M., Ohtake, M., Susuki, N., Yamamoto, Y., Suzuki, K., Tsuji, T. (2014) Ther-
397 mal properties of methane hydrate-bearing sediments and surrounding mud recovered
398 from Nankai Trough wells, *J. Geophys. Res.* 119, 8021-8033.
- 399 Nathues, A., Platz, T., Thangjam, G., Hoffmann, M., Mengel, K., Cloutis, E. A., Le
400 Corre, L., Reddy, V., Kallisch, J., Crown, D. A. (2017) Evolution of Occator Crater on
401 (1) Ceres, *Astron. J.* 153, 112.
- 402 Neveu, M. and S. J. Desch (2015) Geochemistry, thermal evolution, and cryovolcanism on
403 Ceres with a muddy mantle, *Geophys. Res. Lett.* 42, 10,197-10,206.
- 404 Neveu, M., Desch, S., Castillo-Rogez, J., Aqueous chemistry in icy world interiors: Fate
405 of antifreeze and radionuclides, *Geochimica and Cosmochimica Acta* 212, 324-371.
- 406 Opeil, C. P., Consolmagno, C. J., Britt, D. T. (2010) The thermal conductivity of mete-
407 orites: New measurements and analysis, *Icarus* 208, 449-454.
- 408 Park, R., Konopliv, A. S., Bills, B. G., Rambaux, N., Castillo-Rogez, J. C., Raymond, C.
409 A., Vaughan, A. T., Ermakov, A. I., Zuber, M. T., Fu, R. R., Toplis, M. J., Russell, C.
410 T., Nathues, A. (2016) Interior structure of dwarf planet Ceres from measured gravity
411 and shape, *Nature*, accepted.
- 412 Quick, L., Buzckowski, D. L., Ruesch, O. Scully, J. E. C., Castillo-Rogez, J. C.,
413 Raymond, C. A., Schenk, P. M., Sizemore, H. G., Sykes, M. V., A possible brine
414 reservoir below Occator Crater: Thermal and compositional evolution and forma-
415 tion of the Cerealia Dome and Vinalia Faculae, Occator Special Issue of *Icarus*,
416 <https://doi.org/10.1016/j.icarus.2018.07.016>.

- 417 Ruesch O., Platz, T., Schenk, P., McFadden, L. A., Castillo-Rogez, J. C., et al. (2016)
418 Cryovolcanic activity on Ceres, *Science* 353, aaf4286.
- 419 Russell C. T., Raymond C. A., Ammannito E., Buczkowski D. L., De Sanctis M. C.,
420 Hiesinger H., Jaumann R., Konopliv A. S., McSween H. Y., Nathues A., Park R. S.,
421 Pieters C. M., Prettyman T. H., McCord T. B., McFadden L. A., Mottola S., Zuber
422 M. T., Joy S. P., Polanskey C., Rayman M. D., Castillo-Rogez J. C., Chi P. J., Combe
423 J.- P., Ermakov A., Fu R. R., Hoffman M., Jia Y. D., King S. D., Lawrence D. J.,
424 Li J.-Y., Marchi S., Preusker F., Roatsch T., Ruesch O., Schenk P., Villarreal M. N.,
425 Yamashita N. 2016. Dawn arrives at Ceres: Exploration of a small, volatile-rich world.
426 *Science* 353:1008-1010.
- 427 Scully, J. E. C., Buczkowski, D. L., Schmedemann, N., Raymond, C. A., Castillo-Rogez,
428 J. C., King, S. D., Bland, M. T., Ermakov, A. I., O'Brien, D. P., Marchi S., Longobardo,
429 A., Russell, C. T., Fu, R. R., Neveu, M. (2017) Evidence for the Interior Evolution of
430 Ceres from Geologic Analysis of Fractures, *Geophys. Res. Lett.* 44, 9564-9572.
- 431 Sizemore, H., Schmidt, B., Chilton, H., Hughson, K., Castillo-Rogez, J. C., Sori, M.,
432 Platz, T., Buczkowski, D., Berman, D., Ahrens, C., Scully, J., Crown, D., Schenk,
433 P., Mest, S., Bland, M., Otto, K., Marchi, S., Schorghofer, N., Quick, L., Prettyman,
434 T., De Sanctis, M. C., Nass, A., Thangjam, G., Nathues, A., Raymond, C., Russell,
435 C., A Global Inventory of Ice-Related Morphological Features on Dwarf Planet Ceres,
436 <https://doi.org/10.1111/maps.13135>.
- 437 Sori, M. M., Sizemore, H. G., Byrne, S., Bramson, A. M., Bland, M. T., Stein, N. T.,
438 Russell, C. T. (2018) Cryovolcanic rates on Ceres revealed by topography, *Nature As-*

- 439 tronomy, <https://doi.org/10.1038/s41550-018-0574-1>.
- 440 Stein, N. T., Ehlmann, B. L., Palomba, E., De Sanctis, M. C., Nathues, A.,
441 Hiesinger, H., Ammannito, E., Raymond, C. A., Jaumann, R., Longobardo, A., Rus-
442 sell, C. T. (2017) The formation and evolution of bright spots on Ceres, Icarus,
443 <https://doi.org/10.1016/j.icarus.2017.10.014>.
- 444 Sutherland, B. R., Barrett, K. J., Gingras, M. K. (2015) Clay settling in fresh and salt
445 water, *Environmental Fluid Mechanics* 15, 147-160.
- 446 Travis B. J., Bland P., Feldman W. C., and Sykes M. (2018) Hydrothermal dynamics in
447 a CM-based model of Ceres. *Meteoritics & Planetary Science* 53, 2008-2032.
- 448 Waite, W. F., Stern, L. A., Kirby, S. H., Winters, W. J., Mason, D. H. (2007) Simulta-
449 neous determination of thermal conductivity, thermal diffusivity and specific heat in sI
450 methane hydrate, *Geophysical Journal International* 169, 767-774, doi:10.1111/j.1365-
451 246X.2007.03382.x.
- 452 Zambon, F., Raponi, A., Tosi, F., De Sanctis, M. C., McFadden, L. A., Carrozzo, F. G.,
453 Longobardo, A., Ciarniello, M., Krohn, K., Stephan, K., Palomba, E., Pieters, C. M.,
454 Ammannito, E., Russell, C. T., Raymond, C. A. (2017) Spectral analysis of Ahuna Mons
455 from Dawn mission's visible?infrared spectrometer, *Geophys. Res. Lett.* 44, 97-104.

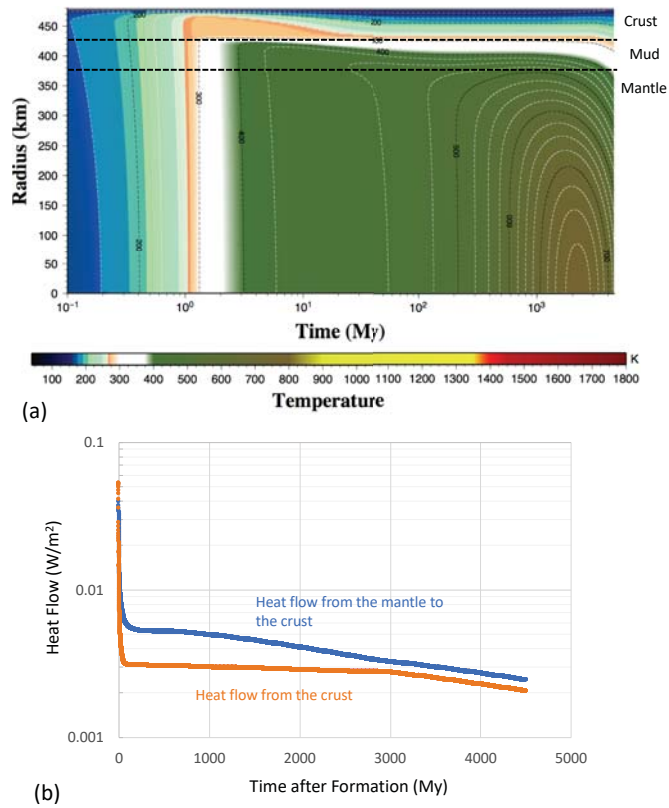


Figure 1. (a) Representative modeling of Ceres' thermal evolution for a time of formation of 3.5 My after the production of Ca-Al inclusions, an averaged crust conductivity of 1.1 W/m/K and mantle thermal conductivity of 1.5 W/m/K. Contour labels are temperatures in Kelvin. The figures display isotherms every 25 K. (b) Corresponding heat flow evolution.

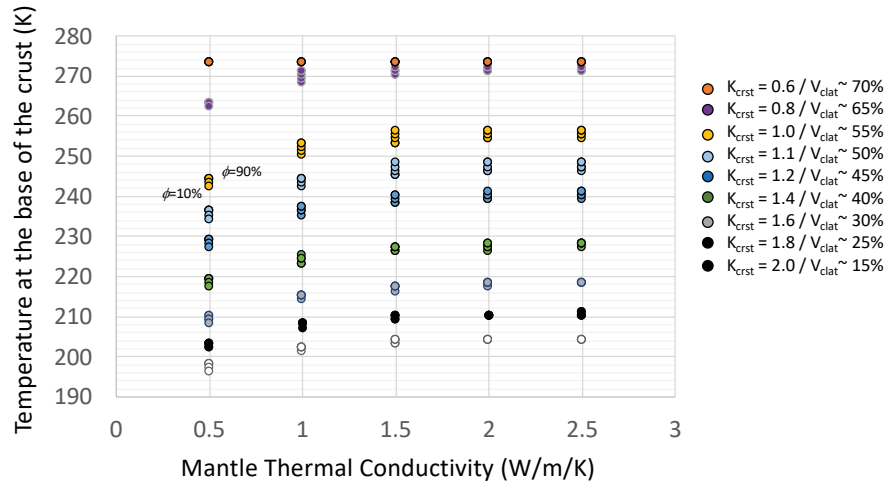


Figure 2. Temperature at the base of the crust as a function of the thermal conductivity in W/m/K of the mantle (assumed constant) and of the crust (temperature dependent, averaged). The corresponding volume fraction of clathrate hydrates in the crust is provided, assuming a mixture of 20 vol.% hydrated salts, 10 vol.%, the rest being ice and clathrates. Point spreads for each model represents the impact of potassium removal from the rock and concentration in a 60 km thick brine layer below the crust, assuming $\phi=0$ to 100% transfer of potassium from the rock to the brine.

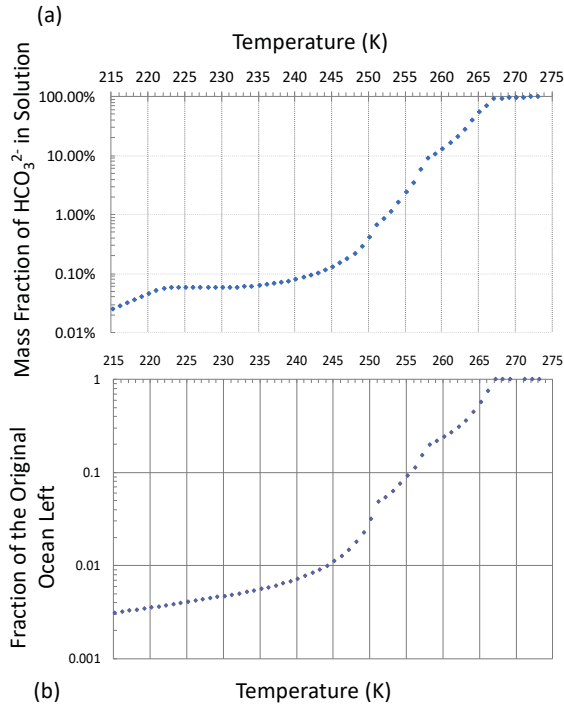


Figure 3. (a) Fraction of liquid left assuming the original ocean was 60 km thick, as a function of the temperature at the base of the crust taking as a reference the ocean composition evolution model from Castillo-Rogez et al. (2018). (b) Fraction of bicarbonate ion in solution as a function of temperature taking as a reference the ocean evolution model from Castillo-Rogez et al. (2018).